Spin transport in the HRSs (JLAB-TN-03-024)

L.Pentchev

June 23, 2003

1 Introduction

Recoil proton polarization experiments using the polarimeter at the focal plane (FPP) of the High Resolution Spectrometer (HRS) in Hall A, require knowledge of the spectrometer spin transport matrix, **S**, to reconstruct the proton polarization at the target. To calculate the matrix **S** one has to use a spectrometer model as an input to a transport code like COSY [1] or SNAKE. Therefore, it is very important to estimate the model dependence of the calculations. The results of the two experiments [2, 3] measuring the proton form-factor ratio $\mu G_e/G_m$ using recoil polarization method, showed decrease of the ratio with Q^2 in contrast to the previous results using Rosenbluth separation. Besides the many advantages of the polarization technique, the result depends on the spectrometer model, and limits of this dependence must be established when comparing the results of the two different methods.

Using the FPP one can measure two components of the proton spin at the focal plane. In contrast, the particle trajectory is known with a good precision before and after the spectrometer and corresponding spectrometer models have been developed as a result of many optical studies. One possible way to investigate the model dependence of the spin matrix calculations is to vary all possible parameters of such models within limits established by the optical studies. The main problem of such procedure is that the spin precession and the trajectory are sensitive to different model parameters. Generally, the procedure is unambiguous. One can achieve agreement with the the optical measurements by varying different model parameters, but the result for the spin transport may be different.

In this work in section 2 we, first, investigate the relation between the trajectory and spin rotation as a particle propagates through a magnetic system. The results of this investigation are applied to the field configuration in the HRS in section 3, and particularly to the case of the proton form-factor ratio experiments in section 4. When calculating the spin matrix, we will introduce step-by-step several approximations and the results after each step will always be compared with the full calculations done with the COSY code. Finally, also in section 4, we describe a procedure for estimating the uncertainties of the spin transport calculations, which is based on results of optical studies of the HRS.

2 Velocity versus. spin propagation

In a magnetic system, the evolution of the the spin ($\vec{P}$) and velocity ($\vec{v}$) are described by the following equations:

$$\frac{d\vec{P}}{dt} = \frac{e}{m\gamma}\vec{P} \times \left[\frac{g}{2}\vec{B}^{\parallel} + \left(1 + \frac{g-2}{2}\gamma\right)\vec{B}^{\perp}\right] \quad (1)$$

$$\frac{d\vec{v}}{dt} = \frac{e}{m\gamma}\vec{v} \times \vec{B}^{\perp} \quad (2)$$

where $\vec{B}^{\parallel}$ and $\vec{B}^{\perp}$ are the field components, respectively, parallel and perpendicular to the velocity, and g is the gyromagnetic ratio.

In the case $\vec{B}^{\parallel} = 0$, the above equations are identical up to a coefficient. If the trajectory is planar, for any bending angle $\Delta\theta$, the spin rotates by an angle, $1 + \gamma(\frac{g}{2} - 1)$ times bigger than $\Delta\theta$. The spin precession angle χ_θ, defined as spin rotation with respect to the velocity is, therefore, equal to:

$$\chi_\theta = \gamma\left(\frac{g}{2} - 1\right)\Delta\theta = f \cdot \Delta\theta \quad (3)$$

In this so called dipole approximation, by measuring the trajectory bending angle, one can reconstruct the spin matrix which for such a simple magnetic system, corresponds to a rotation in the trajectory plane. The amount and the order of the intermediate rotations are not important since in the plane they are additive, and therefore, no model is needed for the spin transport calculations.

In case of non-planar trajectory (but still $\vec{B}^{\parallel} = 0$) the rotations do not commutate and one has to know all the intermediate trajectory rotations in order to calculate the corresponding spin rotations. Let us assume that initially the spin was parallel to the velocity. At a given point along the trajectory specified by the path length s, the spin vector $\vec{P}$ can be defined by the two angles χ_θ and χ_ϕ (Fig. 1) in a local coordinate system in which the l axis is along the velocity, n – in the dispersive direction, and t – in the non-dispersive direction. The angle χ_θ represents spin precession in the dispersive plane, while χ_ϕ – the angle between the spin $\vec{P}$ and its projection on the n-l plane – represents spin precession in the non-dispersive direction. Let us consider trajectory rotation by small angles: $d\theta$ in the dispersive, and $d\phi$ in the non-dispersive direction, respectively. Since rotations by small angles, even in space, are additive, we can apply the dipole approximation in both directions. That means for the above trajectory rotations correspond spin rotations at angles $fd\theta$ and $fd\phi$ in the dispersive and non-dispersive plane, respectively. Then, the change of χ_θ and χ_ϕ is given by:

$$d\chi_\theta = fd\theta + \sin\chi_\theta \sin\phi_s fd\phi \simeq fd\theta \quad (4)$$

$$d\chi_\phi = \cos\left(arctg\frac{tg\chi_\theta}{\cos\phi_s}\right) fd\phi \simeq \cos\chi_\theta fd\phi \quad (5)$$

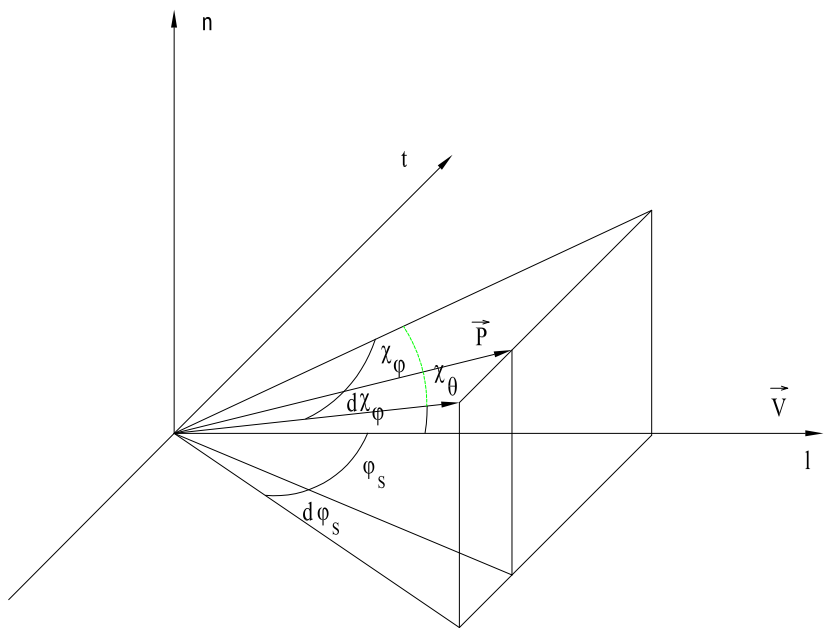

Figure 1: Spin precession in local coordinate system defined by the velocity (l-axis), the n axis being along the dispersive direction, and t - along the non-dispersive one.

where we have assumed that $\phi_s = f\phi$ is small. In this small ϕ_s approximation one can integrate Eqs. (4,5) and separate the precessions in the dispersive and non-dispersive directions explicitly:

$$\chi_\theta(s) = f[\theta(s) - \theta(0)] \tag{6}$$

$$\chi_\phi(s) = \int_0^s \cos\chi_\theta(s) f d\phi(s) = \int_0^s \cos\left(f[\theta(s) - \theta(0)]\right) f d\phi(s) \tag{7}$$

which integrals can be calculated from the trajectory angles $\theta(s)$ and $\phi(s)$.

We define the matrix $\mathbf{S}$ as transformation of the spin from the target $\vec{P}^{tg}$ to the focal plane $\vec{P}^{fp}$ of the spectrometer:

$$\begin{pmatrix} P_n^{fp} \\ P_t^{fp} \\ P_l^{fp} \end{pmatrix} = \begin{pmatrix} S_{nn} & S_{nt} & S_{nl} \\ S_{tn} & S_{tt} & S_{tl} \\ S_{ln} & S_{lt} & S_{ll} \end{pmatrix} \begin{pmatrix} P_n^{tg} \\ P_t^{tg} \\ P_l^{tg} \end{pmatrix} \tag{8}$$

From the precession angles definitions (Fig. 1) we obtain:

$$\begin{aligned} S_{nl} &= \cos\chi_\phi \sin\chi_\theta \\ S_{tl} &= \sin\chi_\phi \\ S_{ll} &= \cos\chi_\phi \cos\chi_\theta \end{aligned} \tag{9}$$

where:

$$\chi_\theta = f[\theta_{fp} - \theta_{tg}] \tag{10}$$

$$\chi_\phi = \int_0^{s_{fp}} \cos\chi_\theta(s) f d\phi(s) \tag{11}$$

and the indexes fp and tg denote the corresponding quantity at the target and at the focal plane, respectively.

Using exactly the same arguments, we calculate the matrix elements that describe the rotation of the normal spin component:

$$\begin{aligned} S_{nn} &= \cos\chi'_\phi \cos\chi_\theta \\ S_{tn} &= -\sin\chi'_\phi \\ S_{ln} &= -\cos\chi'_\phi \sin\chi_\theta \end{aligned} \tag{12}$$

where:

$$\chi'_\phi = \int_0^{s_{fp}} \sin\chi_\theta(s) f d\phi(s) \tag{13}$$

Finally, using the orthogonality we calculate the rotation of the transverse spin component:

$$\begin{aligned} S_{nt} &= S_{tl}S_{ln} - S_{ll}S_{tn} = -\sin\chi_\phi \cos\chi'_\phi \sin\chi_\theta + \cos\chi_\phi \sin\chi'_\phi \cos\chi_\theta \\ S_{tt} &= -S_{ln}S_{nl} + S_{ll}S_{nn} = \cos\chi_\phi \cos\chi'_\phi \\ S_{lt} &= S_{nl}S_{tn} - S_{nn}S_{tl} = -\cos\chi_\phi \sin\chi'_\phi \sin\chi_\theta - \sin\chi_\phi \cos\chi'_\phi \cos\chi_\theta \end{aligned} \tag{14}$$

Note that in small ϕ_s approximation, the matrix $\mathbf{S}$ is orthogonal:

$$\mathbf{S}^T\mathbf{S} = \begin{pmatrix} 1 & 0 & -\sin\chi_\phi \sin\chi'_\phi \\ 0 & \cos^2\chi'_\phi \sin^2\chi_\phi + \cos^2\chi_\phi & 0 \\ -\sin\chi_\phi \sin\chi'_\phi & 0 & 1 \end{pmatrix}$$

because $\chi_\phi < |\phi_s|$ and $\chi'_\phi < |\phi_s|$, as it follows from Eqs. (11,13).

Summarizing, the results in this section were derived (i) in small ϕ_s approximation and (ii) assuming that the longitudinal field component $\vec{B}^{\parallel}$ with respect to the particle trajectory, is zero. If only the second assumption (ii) were valid, then the spin matrix still could be calculated from the particle trajectory angles $\theta(s)$ and $\phi(s)$ without knowing the magnetic field and the absolute position of the trajectory with respect to the optical axis. The first assumption (i) allows us to calculate the matrix elements explicitly as integrals of $\theta(s)$ and $\phi(s)$.

3 Spin propagation in the HRSs

We will apply the results of the previous section to the magnetic field configuration in the HRSs.

In Fig. 2, as an example, we demonstrate the approximation given by Eqs. (9-14) calculated using COSY results for the trajectory angles $\theta(s)$ and $\phi(s)$

for a particular trajectory in HRS. We compare it with numerical calculations assuming only that $\vec{B}^{\parallel} = 0$. In this calculations for each small enough step along trajectory path length s, we rotate the spin at angles of $fd\theta$ and $fd\phi$ that correspond to the trajectory rotations given by $\theta(s)$ and $\phi(s)$ as described in the previous section. For comparison, in the same figure, the COSY results ($\vec{B}^{\parallel}$ not neglected) are shown, calculated also between the magnets.

By comparing the above approximations for different trajectories in HRS as demonstrated in fig. 2 we conclude that the small ϕ_s approximation is very reasonable. The deviations from the full COSY calculations are mainly due to the assumption that $\vec{B}^{\parallel} = 0$. There are two sources of longitudinal field component: the angle of the trajectory with respect to the optical axis to which the main field inside the magnets is perpendicular, and the fringe field at the entrance and exit of the magnets. The analysis show that due to the relatively small angular acceptance the first source is negligible and the fringe fields are the main reason for the deviations from the COSY calculations. The longitudinal field component is most important in the dipole as demonstrated in more details in the bottom panel of Fig. 3 for the S_{tl} matrix element. One can see that the disagreement between the plotted approximations and COSY calculations originates from the dipole region.

The approximation given by Eqs. (9-14) still requires knowledge of the full trajectory, and therefore – model of the spectrometer, since the angles $\theta(s)$ and $\phi(s)$ enter in the integrals (11,13). If, however, we assume that these angles change linearly in the dipole as shown in the two top panels of Fig. 3, the integrals (11,13) can be approximated by the following expressions:

$$\begin{aligned}
\chi_\phi &= \int_0^{s_{fp}} cos\chi_\theta(s) f d\phi(s) \\
&= f\left((\phi_{d1} - \phi_{tg}) + (\phi_{d2} - \phi_{d1})\frac{sin\chi_\theta}{\chi_\theta} + (\phi_{fp} - \phi_{d2})cos\chi_\theta\right) \qquad (15) \\
\chi'_\phi &= \int_0^{s_{fp}} sin\chi_\theta(s) f d\phi(s) \\
&= f\left((\phi_{d2} - \phi_{d1})\frac{1 - cos\chi_\theta}{\chi_\theta} + (\phi_{fp} - \phi_{d2})sin\chi_\theta\right) \qquad (16)
\end{aligned}$$

where ϕ_{d1}, ϕ_{d2} are the non-dispersive angles before and after the dipole. These two angles can be calculated from the trajectory parameters at the target and at the focal plane by modeling only the quadrupoles and excluding the dipole which is the most delicate part of the HRS model. The results of the above approximation (15,16) are demonstrated in the bottom panel of Fig. 3 and in Fig. 2.

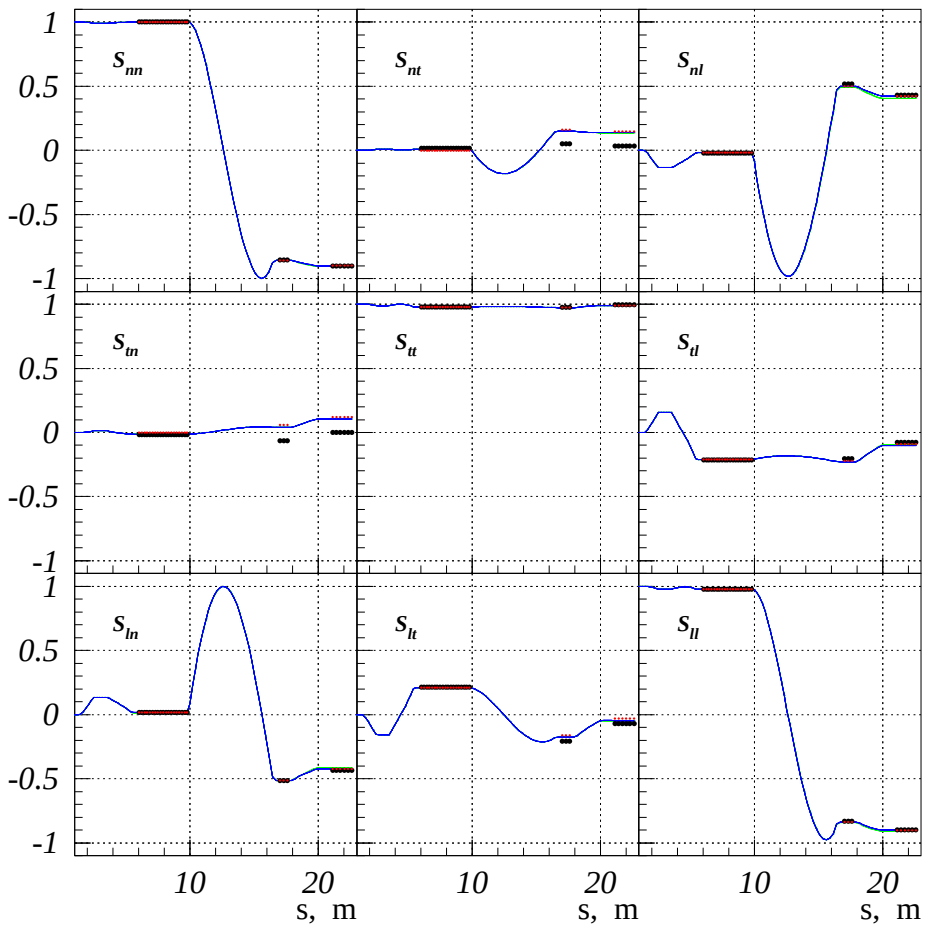

Figure 2: Evolution of the spin matrix element along the trajectory path length s calculated as follows: blue line – small ϕ_s and $\vec{B}^{\parallel} = 0$ approximation (9-14); green line (plotted but almost indistinguishable from blue curves) – $\vec{B}^{\parallel} = 0$ approximation, numerical integration; red points – linear angle change approximation (15,16); black points – full COSY calculations. For trajectory defined by $\theta_{tg} = 30mrad$, $p = p_0 = 2.05GeV/c$, $y_{tg} = 0$, $\phi_{tg} = 30mrad$.

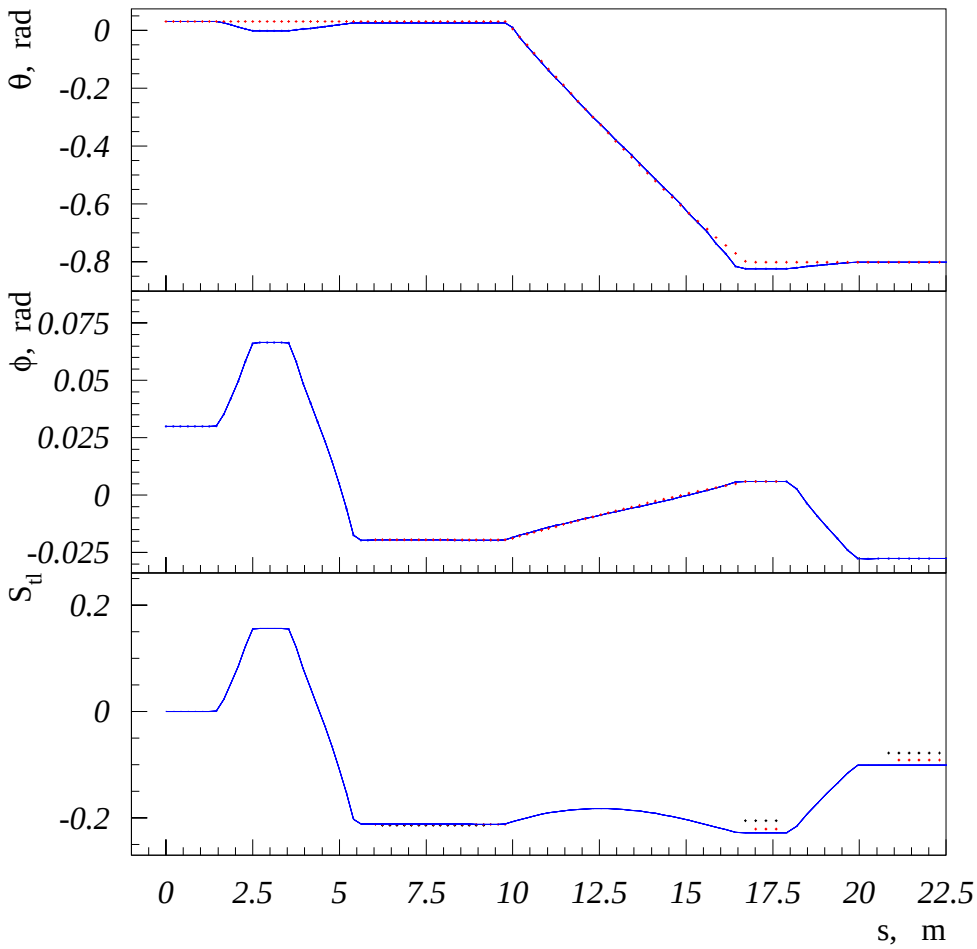

Figure 3: Trajectory angles θ (top) and ϕ (middle) for $\theta_{tg} = 30mrad$, $p = p_0 = 2.05GeV/c$, $y_{tg} = 0$, $\phi_{tg} = 30mrad$; and S_{tl} (bottom) calculated with COSY (black), approximation (9-14) (blue), and approximation (15,16) (red) the later corresponding to the assumption about angles $\theta(s)$ and $\phi(s)$ as shown with red on the two top panels; all as functions of the trajectory path length s.

4 Application to the proton form-factor ratio measurements

In case of elastic $\vec{e}p$ scattering in one photon exchange approximation, there is no normal component of the proton polarization at the target, therefore for the two polarization components that can be measured at the focal plane we obtain from Eq. (8):

$$\begin{aligned} P_n^{fp} &= S_{nt}P_t^{tg} + S_{nl}P_l^{tg} \\ P_t^{fp} &= S_{tt}P_t^{tg} + S_{tl}P_l^{tg} \end{aligned} \tag{17}$$

For the matrix elements in the above equations we use the approximation from the previous section defined by Eqs. (9-14). In addition we neglect all the terms containing χ_ϕ and χ'_ϕ of order two and higher as negligible in the small ϕ_s approximation. Then, the solution of Eq. (17) is given by:

$$\begin{aligned} P_t^{tg} &= -\frac{\chi_\phi P_n^{fp}}{sin\chi_\theta} + P_t^{fp} \\ P_l^{tg} &= \frac{1}{sin\chi_\theta}\left(P_n^{fp} + (\chi_\phi sin\chi_\theta - \chi'_\phi cos\chi_\theta)P_t^{fp}\right) \end{aligned} \tag{18}$$

In the Q^2 region of $0.5 - 5.6$ GeV^2 P_t^{tg} is $3 - 10$ times smaller than P_ℓ^{tg}. Since χ_ϕ and χ'_ϕ are small, we can neglect $(\chi_\phi sin\chi_\theta - \chi'_\phi cos\chi_\theta)P_t^{fp}$ in comparison to P_n^{fp} in the last equation. Then we rewrite the above set of equations in the form:

$$\frac{P_t^{tg}}{P_l^{tg}} = \frac{P_t^{fp}}{P_l^{tg}} - \chi_\phi \tag{19}$$

$$P_l^{tg} = \frac{P_n^{fp}}{sin\chi_\theta} \tag{20}$$

The elastic form factor ratio is proportional to the ratio of the polarization components at the target [4]:

$$\frac{G_{Ep}}{G_{Mp}} = -\frac{P_t^{tg}}{P_\ell^{tg}}\frac{(E+E')}{2m_p}\tan(\frac{\theta_e}{2}) \tag{21}$$

and therefore, proportional to the right-hand side of Eq. (19). Here, E, E' and θ_e are the initial, final electron energy, and the scattering angle, respectively. Thus, the form factor ratio is very sensitive to χ_ϕ, in contrast to $sin\chi_\theta$ which is multiplied by a small term P_t^{fp}/P_n^{fp} after substituting P_l^{tg} from Eq. (20) in Eq. (19). Eq. (19) also means that by measuring the polarization components at the focal plane as functions of different trajectory parameters one can study the dependence of χ_ϕ on these parameters, since the polarization components at the target don't depend on them. This is demonstrated bellow.

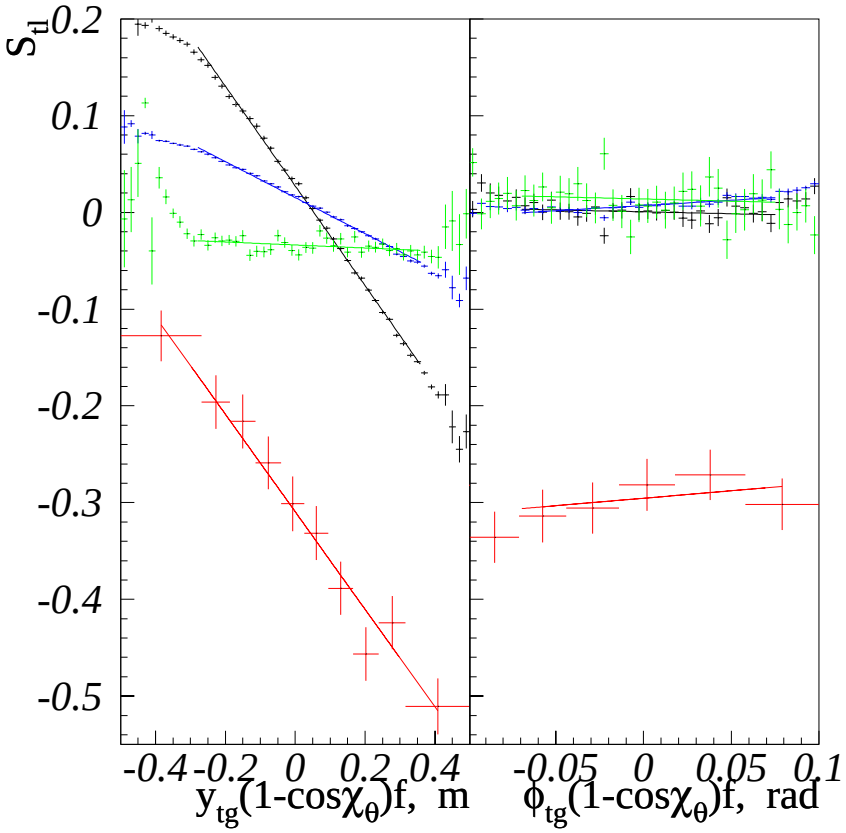

Figure 4: P_t^{fp}/P_l^{tg} (red) reconstructed from the data at $Q^2 = 2.13$ GeV^2 compared with the matrix element S_{tl} calculated with COSY (black), and its contributions: $f(\phi_{fp} cos\chi_\theta - \phi_{tg})$ (blue), q_ϕ (left panel, green), and q_y (right panel, green); in bins of q_y (left panel) and q_ϕ (right panel) and fitted with straight lines.

Equations (15, 16) can be rewritten in the form:

$$\begin{aligned}\chi_\phi &= f[(\phi_{fp}cos\chi_\theta - \phi_{tg}) \\ &+ \phi_d(1-cos\chi_\theta) - \Delta\phi_d(1 - \frac{2sin\chi_\theta}{\chi_\theta} + cos\chi_\theta)] \qquad (22)\\ \chi'_\phi &= f\left[\phi_{fp}sin\chi_\theta - \phi_d sin\chi_\theta + \Delta\phi_d\left(\frac{2(1-cos\chi_\theta)}{\chi_\theta} - sin\chi_\theta\right)\right] \qquad (23)\end{aligned}$$

where $\phi_d = (\phi_{d2} + \phi_{d1})/2$ is the mean angle in the dipole, and $\Delta\phi_d = (\phi_{d2} - \phi_{d1})/2$ – half of the bend angle in the dipole in non-dispersive direction. Note that in Eq. (22), in the region of $\chi_\theta \sim 180^0$ the ϕ_d term is dominant while the $\Delta\phi_d$ one is negligible and vice versa in the region of $\chi_\theta \sim 360^0$. In first order these angles depend only on the non-dispersive target coordinate and angle:

$$\begin{aligned}\phi_d &= (\phi_d|y_{tg})y_{tg} + (\phi_d|\phi_{tg})\phi_{tg} \qquad (24)\\ \Delta\phi_d &= (\Delta\phi_d|y_{tg})y_{tg} + (\Delta\phi_d|\phi_{tg})\phi_{tg} \qquad (25)\end{aligned}$$

To calculate the above couplings we take the derivative of Eq. (19) in which χ_ϕ is replaced by Eq. (22), with respect to the following quantities:

$$\begin{aligned}q_y &= y_{tg}(1-cos\chi_\theta)f \\ q_\phi &= \phi_{tg}(1-cos\chi_\theta)f\end{aligned} \qquad (26)$$

and since P_l^{tg} and P_t^{tg} do not depend on them we obtain:

$$\begin{aligned}(\phi_d|y_{tg}) &= \frac{1}{P_l^{tg}}\frac{\partial P_t^{fp}}{\partial q_y} - \frac{\partial}{\partial q_y}f(\phi_{fp}cos\chi_\theta - \phi_{tg}) - (\phi_d|\phi_{tg})\frac{\partial q_\phi}{\partial q_y} \\ &+ \frac{\partial}{\partial q_y}f\Delta\phi_d(1 - \frac{2sin\chi_\theta}{\chi_\theta} + cos\chi_\theta) \\ (\phi_d|\phi_{tg}) &= \frac{1}{P_l^{tg}}\frac{\partial P_t^{fp}}{\partial q_\phi} - \frac{\partial}{\partial q_\phi}f(\phi_{fp}cos\chi_\theta - \phi_{tg}) - (\phi_d|y_{tg})\frac{\partial q_y}{\partial q_\phi} \\ &+ \frac{\partial}{\partial q_\phi}f\Delta\phi_d(1 - \frac{2sin\chi_\theta}{\chi_\theta} + cos\chi_\theta) \qquad (27)\end{aligned}$$

To estimate the couplings $(\phi_d|y_{tg})$ and $(\phi_d|\phi_{tg})$, we use the experimental data for $Q^2 = 2.13GeV^2$. In Fig.4 we plot P_t^{fp}/P_l^{tg} and the mean values of $f(\phi_{fp}cos\chi_\theta - \phi_{tg})$, q_y and q_ϕ in bins of q_y and q_ϕ. Note that all these quantities are reconstructed from the experimental data without using any spectrometer model, in particular P_l^{tg} is calculated from Eq. (20). One can see (green crosses in Fig.4) that in the above equations, the contributions of the terms containing $\partial q_\phi/\partial q_y$ and $\partial q_y/\partial q_\phi$ are small. In the same way it can be demonstrated that the last terms in the above two equations are negligible. This is true in a wide region around $\chi_\theta \sim 180^0$ ($Q^2 = 2.13GeV^2$). Therefore, the above couplings are calculated by fitting the slopes of P_t^{fp}/P_l^{tg} and $f(\phi_{fp}cos\chi_\theta - \phi_{tg})$ and subtracting them.

For comparison, in Fig.4 we also show S_{tl} calculated with COSY. According to Eq. (19) the slope of P_t^{fp}/P_l^{tg} as reconstructed from the experimental data, and the slope of the matrix element $S_{tl} \approx \chi_\phi$ must be similar, so that the ratio of the polarization components at the target do not depend on q_y and q_ϕ. Essentially, this property is used in the above procedure to calculate the couplings $(\phi_d|y_{tg})$ and $(\phi_d|\phi_{tg})$. The results we obtain, $(\phi_d|y_{tg}) = -0.317 \pm 0.038$ and $(\phi_d|\phi_{tg}) = -0.066 \pm 0.082$, are similar to the couplings calculated with COSY: $(\phi_d|y_{tg}) = -0.368$ and $(\phi_d|\phi_{tg}) = -0.152$.

Similarly, working in the region of $\chi_\theta \sim 360^0$ ($Q^2 = 5.6GeV^2$) and plotting the same quantities in bins of

$$
\begin{aligned}
q'_y &= -y_{tg}(1 - \frac{2sin\chi_\theta}{\chi_\theta} + cos\chi_\theta)f \\
q'_\phi &= -\phi_{tg}(1 - \frac{2sin\chi_\theta}{\chi_\theta} + cos\chi_\theta)f
\end{aligned}
$$

we reconstruct the other two couplings: $(\Delta\phi_d|y_{tg}) = 0.218 \pm 0.105$ and $(\Delta\phi_d|\phi_{tg}) = -0.287 \pm 0.111$. These couplings are important only in the region of $\chi_\theta \sim 360^0$ where the term in Eq. (22) containing $\Delta\phi_d$ is not negligible.

Having the above couplings reconstructed, we are ready to use the spin matrix approximation given by Eqs. (9,12,14) in which the precession angles are calculated from Eq. (10) and Eqs. (22,23). All these equations depend only on the dispersive and non-dispersive bend angles in the spectrometer $(\theta_{fp} - \theta_{tg})$ and $(\phi_{fp} - \phi_{tg})$ and on the proton γ-factor, except for the angles ϕ_d and $\Delta\phi_d$, calculated from Eqs. (24,25) using the reconstructed couplings.

In figures 5, 6, 7, and 8 the results of this approximation are compared event-by-event with the COSY calculations for the data from the proton form-factor experiments E93-027 and E99-007. One can see that the agreement is fairly good over the whole range of χ_θ from 90^0 to 390^0. It can be demonstrated that the precession angle χ_ϕ is always smaller than χ'_ϕ and the Eqs. (14) can be simplified by neglecting the terms containing $\sin\chi'_\phi$, in which case the results are very similar to those shown at figures 5, 6, 7, and 8.

By means of this approximation we can formulate a prescription for estimating the systematic errors of physical quantities that depend on the spin matrix elements. We separate the systematic errors into two types: (i) the ones coming from the uncertainties using the above approximation, and (ii) the errors on the corrections to that approximation. To estimate the first contribution, one varies all the experimental quantities that enter in the above approximation:

- the bend angles $\theta_{fp} - \theta_{tg}$ and $\phi_{fp} - \phi_{tg}$, and the momentum p, within the limits estimated from the optical studies of the HRS
- the reconstructed couplings $(\phi_d|y_{tg})$, $(\phi_d|\phi_{tg})$, $(\Delta\phi_d|y_{tg})$, and $(\Delta\phi_d|\phi_{tg})$, within the errors stated above

and calculates the corresponding error on the physical quantity. To reduce the systematic errors one has to minimize the uncertainties in the above quantities. In case of the $\mu G_e/G_m$ data, it turns out that the form factor ratio is especially

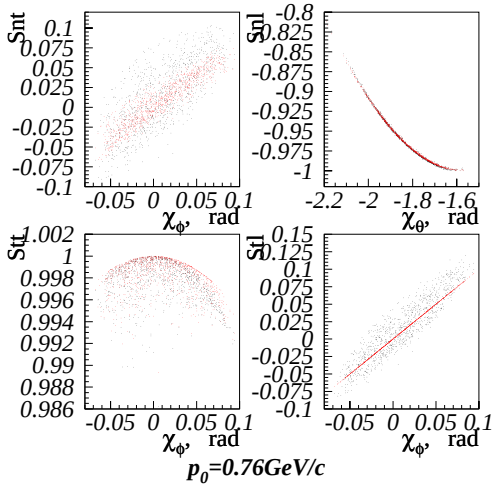

Figure 5: Spin matrix elements calculated with COSY (black) and approximation given by Eqs. (9,12,14) in which the precession angles are calculated from Eqs.(10,22,23) using the reconstructed coupling constants (red); as functions of the precession angles χ_θ and χ_ϕ for central proton momentum of 0.76 GeV/c ($Q^2 = 0.49$ GeV^2).

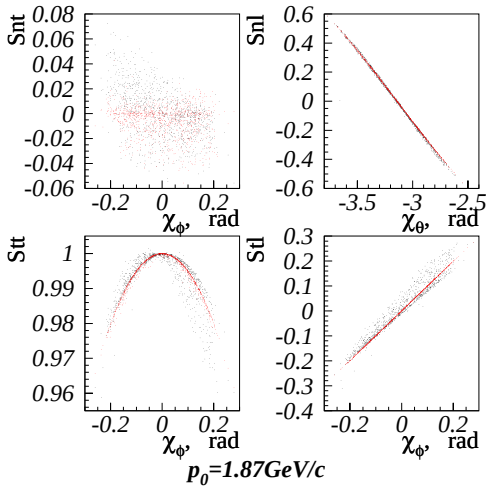

Figure 6: Same as Fig. 4 for central proton momentum of 1.87 GeV/c ($Q^2 = 2.13$ GeV^2).

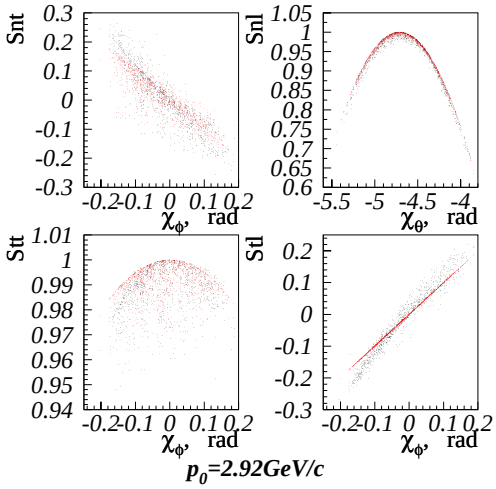

Figure 7: Same as Fig. 4 for central proton momentum of 2.92 GeV/c ($Q^2 = 4.0$ GeV^2).

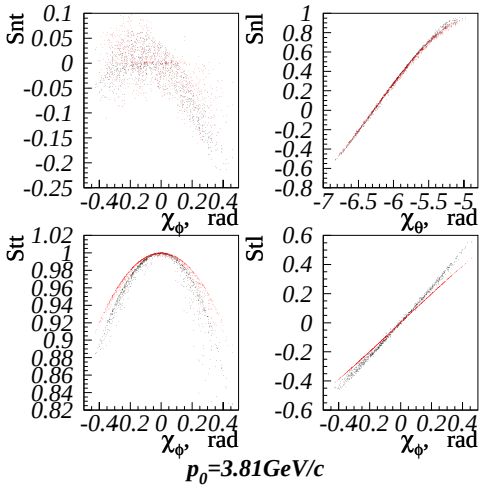

Figure 8: Same as Fig. 4 for central proton momentum of 3.81 GeV/c ($Q^2 = 5.6$ GeV^2).

sensitive to the non-dispersive bend angle $\phi_{fp} - \phi_{tg}$. In devoted optical studies [5] we achieved 0.3 mrad precision for the non-dispersive bend angle of the central trajectory. As for the dispersive bend angle, such a good precision is not needed. Plotting the P_n^{fp} polarization component in bins of the dispersive precession angle χ_θ and measuring the zero crossing points at $\chi_\theta \sim 180^0$ and $\chi_\theta \sim 360^0$, from Eq. (10) we reconstructed the absolute value of the dispersive bend angle with a precision of 3 mrad for the right HRS and 4.4 mrad for the left HRS.

The second contribution to the systematics can be estimated by comparing the calculations done with the above approximation and with the COSY model. By varying different focal plane and target quantities, and model parameters the results from both calculations change because effectively we change the quantities listed in the previous paragraph, however the change of the difference between the two calculations (i.e. the change of the correction to the spin matrix approximation) gives us the second contribution to the systematic errors. In case of the $\mu G_e/G_m$ data, the spin matrix approximation and the full COSY calculations give very similar results. The variation of the difference between the two calculations is even smaller and negligible as compared with the first type of systematic errors.

5 Conclusions

The HRS spin matrix is in good approximation a function mainly of the momentum p, and the total trajectory bending angles in dispersive and non-dispersive directions: $\theta_{fp} - \theta_{tg}$, $\phi_{fp} - \phi_{tg}$. While, the momentum is known with sufficiently high precision, special measurements are required to achieve good precision for the total bending angles. The bending of the trajectory in the non-dispersive direction from the target to the dipole and within the dipole, on which the spin matrix depends as well, don't need to be known with high precision and can be reconstructed from elastic $\vec{e}p -> e\vec{p}$ measurements. The approximation will not work for spectrometers with strong fringe field effects, where these effects are the main reason for the deviation of this approximation from the COSY calculations.

6 Acknowledgments

I would like to thank my colleagues O. Gayou, M. Jones, C.Perdrisat, and V. Punjabi for their support in all the stages of analyzing the systematics of the $\mu G_e/G_m$ experiments and for the fruitful discussion of this work.

References

[1] K.Makino and M. Bertz, COSY INFINITY version 8, Nucl. Inst. and Meth.**A427**, 338 (1999).

[2] M. K. Jones *et al.*, Phys. Rev. Lett. **84**, 1398 (2000).

[3] O. Gayou *et al.*, Phys. Rev. Lett. **88** 092301 (2002)

[4] A.I. Akhiezer and M.P. Rekalo, Sov. J. Part. Nucl. **3**, 277 (197 4).

[5] L. Pentchev and J.J. Lerose, "Quadrupole alignment studies in the HRSs" JLab-TN-01-052, 2001.